Positioning with Chinese DTMB Signal under Complex Urban Environments

Tao Zhou, Liang Chen *

State Key Laboratory of Information Engineering in Surveying, Mapping and Remote Sensing (LIESMARS).
Wuhan University, Hubei Province. China.
Email: l.chen@ whu.edu.cn

Keywords: Chinese Digital Multimedia Broadcast (DTMB), Non-GNSS-based PNT Solutions, Wireless positioning, Orthogonal frequency division multiplexing (OFDM).

Abstract

With the development of the Global Navigation Satellite System (GNSS), the GNSS can provide a wide-area positioning, navigation, and timing (PNT) service. However, the GNSS can not work well in some environments, such as GNSS jamming environments and GNSS denied environments. Thus, it is necessary to develop a non-GNSS-based PNT solution. Chinese digital multimedia broadcast (DTMB) signal presents a potential opportunity for wireless localization. In this paper, we proposed a software-defined radio (SDR) receiver based on the DTMB signal for positioning. The key innovations of the proposed SDR receiver are as follows: 1) proposing a fusion filter to fuse the information from the frequency-locked loop (FLL), and phase-locked loop (PLL) to improve the performance of the PLL under high dynamical environments; 2) utilizing the carrier-to-noise radio (C/N0) to remove the range observation influenced by heavy non-line of sight (NLOS) environment and utilizing the usable range observations for positioning. To evaluate the performance of the designed DTMB receiver, a series of field experiments are conducted. The pedestrian experiment results show that the $1-\sigma$ ranging error from the carrier phase is about 0.94m. The on-vehicle experiment results show that the $1-\sigma$ positioning error in the eastward is about 9.07m, and the $1-\sigma$ positioning error in the northward is about 7.74m. This means the designed DTMB receiver can provide sub-meter ranging results under pedestrian environments, and the proposed DTMB receiver is able to provide meter-level positioning results under complex urban environments. Related research shows that the signal point position method (SPP) of GNSS also provides meter-level positioning results under complex urban environments. Thus, the proposed DTMB receiver can be utilized as a non-GNSS-based PNT solution.

1. Introduction

The Global Navigation Satellite System (GNSS) can provide a wide-area positioning, navigation, and timing (PNT) service, and it has had a widely application on mobile robots, vehicles, and other automatic navigation systems. However, the GNSS can not work well in some environments, such as GNSS jamming environments and GNSS denied environments. Thus, it is necessary to develop a non-GNSS-based PNT solution, and terrestrial television signals have been designed for both indoor and outdoor reception. Recently, wireless positioning using Chinese digital multimedia broadcast (DTMB) signals has garnered increasing interest, particularly after the widespread deployment of DTMB systems for a large user base (Wu et al., 2006, Zhang et al., 2015). It has been recognized that the DTMB signals can be used for positioning (Chen et al., 2015). Compared with the GNSS, there are advantages for the positioning based on the DTMB signal (Chen et al., 2015, Chen et al., 2016):

- DTMB signals are transmitted with a higher power, and their frequency band ranges from 400-700 MHz, providing better building penetration and urban propagation than GNSS signals, which operate at approximately 1-3 GHz.
- The nominal signal bandwidth of the digital multimedia broadcast signals is designed between 6-8 MHz, which is wider than that of GNSS signals. This will improve the signal synchronization accuracy, leading to more precise pseudo-range measurements.
- DTMB stations are fixed, and the receivers typically exhibit very slow movement, resulting in minimal Doppler effects compared to GNSS signals.
- The relatively stable distance between DTMB stations and receivers minimizes the impact of ionospheric and tropospheric delays, which significantly affect GNSS signals. This will lead to easier signal acquisition and the possibility of integration over a longer period.
- It is unable to provide the available positioning results based on the GNSS signal in the GNSS jamming environments, such as some battle areas. However, if the DTMB signal is not jammed, the DTMB signal can be utilized for positioning.

As a signal of opportunity (SoO) for positioning, the DTMB facilities have already been developed, and there is no need to build extra infrastructure investments, except for the positioning devices. Based on these facts, using the DTMB system for positioning has attracted more and more researchers. The methods using DTMB system for positioning include ranging-based positioning methods and fingerprinting-based methods. The ranging-based methods include DTMB-aided GNSS positioning methods (Jiao et al., 2023), DTMB-aided IMU (Inertial Measurement Unit) methods (Liu et al., 2022a) and DTMB-aided other OFDM, such as LTE (Long Term Evolution), positioning methods (Hong et al., 2021). For the research of the DTMB-aided GNSS positioning methods, the reference (Jiao et al., 2023) is representative. In the reference (Jiao et al., 2023), Jiao, Z et al. proposed a method that utilizes the carrier phase ranging with DTMB signals and GNSS for pedestrian positioning. The experiments show that the ranging accuracy of the

* Corresponding author

carrier phase is 0.04m in the static scenario, and the ranging accuracy of the carrier phase is 2.2m in the dynamical scenario. For the research of the DTMB-aided IMU methods, the reference (Liu et al., 2022a) is representative. In the reference (Liu et al., 2022a), X. Liu et al. proposed an enhanced pedestrian dead reckoning (PDR) aided with DTMB signals. The field experiments show that the 95% positioning error of the proposed algorithm is less than 3.94 m, while the PDR only is less than 9.19 m. About the research of the DTMB-aided other OFDM methods, the reference (Hong et al., 2021) is well. In the reference (Hong et al., 2021), T. Hong et al. proposed the hybrid positioning with DTMB and LTE signals method. The experiments show that the proposed method in (Hong et al., 2021) can provide an RMSE of 20.45m over a trajectory of 600m. About the fingerprinting-based methods, Wu, H et al. (Wu et al., 2016) proposed a positioning method based on the FM radio and DTMB signals fingerprinting, and the experiment shows that DTMB fingerprinting has a wider coverage area, a lower maintenance cost, and more stable signal strength. These researches have shown that the DTMB signal has a good positioning performance, but they did not analyze the positioning performance of the DTMB-only methods. Thus, we proposed a DTMB receiver for positioning in this paper. The contribution of this paper is as follows.

- A fusion filter is proposed to fusion the information from the frequency-locked loop, and phase-locked loop to improve the performance of the phase-locked loop (PLL) under high dynamical environments.
- The carrier-to-noise radio (C/N0) is used to remove the range observation influenced by the heavy non-line of sight (NLOS) environment and utilize the cleared range observation for positioning.

The paper is organized as follows: Section II describes the DTMB signal standard and the signal model. Section III describes the receiver design, including acquisition and tracking. Section IV describes the DTMB localization framework. The experiment setup and receiver configuration has been discussed in Section V. A pedestrian experiment has been conducted in Section VI. Section VII discusses the results of the on-vehicle experiment. Finally, conclusions are summarized in Section VIII

2. DTMB Standard and the Signal Structure

The DTMB signals use the OFDM (orthogonal frequency division multiplexing) modulation to achieve robust transmission in multipath scenarios. In DTMB signals, OFDM signals contain the frame head and frame body. The frame head contains the PN (Psudo-Range Noise) sequence, and it is in the OFDM guard interval. The frame body includes the transmitted data, such as video, message, audio, etc (Jiao et al., 2023). In the DTMB system, signals are continuously transmitted, and every OFDM symbol is transmitted within a fixed duration. Every OFDM symbol contains a PN frame. From the wireless position, the good autocorrelation property of the PN and the continuous transmission are helpful for accurately tracking signals for TOA estimation.

The PN in DTMB signals mainly includes three structures, which are shown in Tab 1. For model 1 and model 3, the PN sequences can be mapped to each subcarrier of the OFDM signal. For model 2, due to the fact that there is no shift property for the PN sequence, it cannot be mapped to all subcarriers of the OFDM signal. Due to there being better multipath resistance for the multicarrier modulation, the signals in model 1 and model 3 are frequently used. (Jiao et al., 2023).

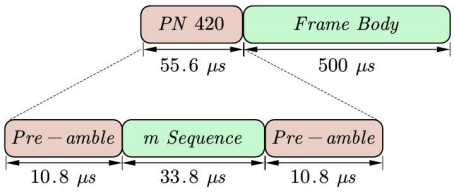

(a) DTMB Signal in Model 1

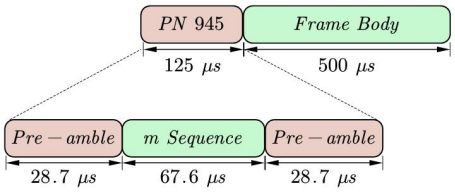

(b) DTMB Signal in Model 3

Figure 1. DTMB Signal Structure

Table 1. PN Structures of DTMB signal

PN Model	Description
Model 1	Header Frame Symbols (420), Duration (55.6μs)
Model 2	Header Frame Symbols (595), Duration (78.7μs)
Model 3	Header Frame Symbols (945), Duration (125μs)

The DTMB signal structures of model 1 and model 3 are shown in Fig 1. The Fig 1 described the DTMB signals in model 1 and model 3. The frame head of the DTMB signal in model 1 is defined as PN 420, and the frame head of the DTMB signal in model 3 is defined as PN 945, which is according to the sample number of the frame head. The frame head includes a pre-amble sequence, a post-amble sequence, and an m sequence. The pre-amble sequence and the post-amble sequence are the same. Thus, we can utilize the specificity to realize the rough acquisition. For the DTMB signal in model 1, the sample number of the pre-amble sequence and the post-amble sequence is 82, and the sample number of the m sequence is 256. About the DTMB signal in model 3, the sample number of the pre-amble sequence and the post-amble sequence is 217, and the number of the m sequence is 511. For the DTMB signal in model 1, the preamble sequence is the copy of the first 82 samples for the m sequence, and the post-amble sequence is the copy of the last 82 samples for the m sequence. About the DTMB signal in model 3, the preamble sequence is the copy of the first 217 samples for the m sequence, and the post-amble sequence is the copy of the last 217 samples for the m sequence. The generator polynomial for the m sequence in model 1 is $G_{420} = 1 + x + x^5 + x^6 + x^7$, and the generator polynomial for the m sequence in model 3 is $G_{945} = 1 + x^2 + x^7 + x^8 + x^9$.

The transmitted time-domain signal is affected by the multipath, the frequency offset that is caused by the difference between the transmitter and the receiver oscillators, and the Doppler effect caused by the relative motion between the transmitter and

the receiver. The received signal can be modeled as

$$r[n] = A(t)\widetilde{s}_T[t-\tau(t)]e^{j[2\pi f_D(t)+\phi(t)]}|_{t=kT_s} + n(t)|_{t=kT_s} \quad (1)$$

where $r[n]$ denotes the received signal, and $\widetilde{s}_T(t)$ denotes the transmitted data. $\tau(t)$ represents the timing delay, $f_D(t)$ represents the frequency offset caused by the sampling frequency offset and the Doppler effect due to the relative motion. $\phi(t)$ is a timing-varying carrier phase shift, and $n(t)$ is a term modeling random noise. T_s denotes the sampling period.

3. Receiver Design

The receiver proposed in the paper mainly consists of the acquisition and tracking. When the receiver is started, the DTMB baseband signal is processed in the acquisition part to roughly estimate the timing delay and frequency offset. After the acquisition is finished, the DTMB baseband signal will be processed in the tracking part. The role of the tracking part is to precisely estimate the timing delay, frequency offset, and carrier phase. The tracking part continuously receives the signal until the signal lock is lost. When the signal lock is lost, the DTMB baseband signal will be processed in the acquisition part until the acquisition is finished. Then, the DTMB baseband signal will be processed again in the tracking part. The overview of the proposed receiver is shown in Fig 2.

3.1 Acqusition Stage

In this section, we discussed the acquisition of the proposed receiver. The main work during the acquisition stage is to estimate the rough timing delay and the rough frequency offset. Without the high relative motion between the transmitter and the receiver and the high difference between the transmitter and the receiver oscillators, the frequency offset is normally relatively little. It means that the frequency offset does not have an obvious influence on the timing estimation, so we can estimate timing estimation before estimating frequency offset (Liu et al., 2022b). The principle of estimating the rough timing delay is to cross-correlate the local template and the received signal and find the location of the maximum correlation value. The location of the maximum correlation value is the estimated timing delay, and the process of estimating the timing delay can be modeled as

$$\Phi_0 = \arg\max_k |\sum_{n=0}^{N_{PN}-1} r(n+k)\cdot s^*_{local}(n)|, \quad k = 0,1,2,...,N_{frame}-1 \quad (2)$$

where Φ_0 denotes the estimated rough timing delay, which represents the location of the max peak in the correlation sequence. $r(n+k)$ denotes the received signal, and $s^*_{local}(n)$ denotes the local PN sequence. N_{PN} represents the length of the PN sequence, and N_{frame} represents the length of a frame. The principle for the calculation of the frequency offset is to obtain the difference of the carrier phases between the neighbor frames, and it can be calculated as

$$\Delta f_k = \frac{1}{2\pi T_\eta} atan2(I_{P,k-1}Q_{P,k} - Q_{P,k-1}I_{P,k}, I_{P,k-1}I_{P,k} + Q_{P,k-1}Q_{P,k}) \quad (3)$$

where Δf_k denotes the estimated frequency offset. $R_{p,k} = I_{P,k} + jQ_{P,k}$ represents the correlation values between the PN sequence of the kth received signal frame and the corresponding local PN sequence, and the $R_{p,k}$ can be modeled as

$$R_{p,k} = \sum_{n=0}^{N_{PN}-1} r_{PN}(n)\cdot s^*(n) \quad (4)$$

3.2 Tracking Stage

After the acquisition stage, the tracking stage commences. Continuous signal tracking is realized by using a closed-loop architecture. Keeping tracking signals continuously is mainly for two reasons: 1) to produce pseudorange measurements; 2) to reconstruct the carrier continuously. The main components of the tracking loop include a frequency-locked loop (FLL)- assisted phase-locked loop (PLL), a carrier-aided delay-locked loop (DLL), a loop filter, and a numerically-controlled oscillator (NCO).

(1) FLL-Assisted PLL: Under high dynamical stress, there is better performance for FLL than PLL. However, PLL has higher measurement accuracy than FLL. An FLL-assisted-PLL has both high robustness under high dynamical stress and high measurement accuracy (Yang et al., 2022). The main components of the FLL-assisted-PLL are an FLL discriminator, a PLL discriminator, and an FLL-assisted-PLL loop filter. In this paper, the FLL-assisted-PLL loop filter is the first layer of the loop filter, which is shown in Fig. 2. In this part, the FLL discriminator and the PLL discriminator will be discussed.

The range of the *atan2* discriminator estimation is $\pm\pi$, which can be used to decrease the risk of introducing phase ambiguities. In this paper, we use *atan2* discriminator for FLL discriminator and PLL discriminator. The FLL discriminator can be expressed as

$$e_{FLL} = \frac{atan2(Q_{p,k}, I_{p,k}) - atan2(Q_{p,k-1}, I_{p,k-1})}{2\pi T_\eta} \quad (5)$$

where $R_{p,k} = I_{p,k} + jQ_{p,k}$ is the prompt correlation at time step k, and T_η is the period between the neighbor frames. T_η is normally equals with $N_{frame}\frac{1}{f_r}$, N_frame represents one frame length and f_r represents the sample rate. The PLL discriminator is expressed as

$$e_{PLL} = atan2(Q_{p,k}, I_{p,k}) \quad (6)$$

2) DLL: We used the Early-Minus-Late Power Delay Discriminator (EML) to obtain the DLL estimation. The EML can be expressed as

$$e_{DLL} = \frac{1}{k(\xi)}(|R(-\xi)|^2 - |R(\xi)|^2) \quad (7)$$

where e_{DLL} represents the code phase error estimated by nEML. The normalized factor $k(\xi)$ is used to keep $e_{DLL} \approx \epsilon$. $|R(-\xi)|^2$ denotes the early power and $|R(\xi)|^2$ denotes the late power. The early power $|R(-\xi)|^2$ and late power $|R(\xi)|^2$ are expressed as

$$|R(\mp\xi)|^2 = \sum_{n=0}^{N_{PN}-1} \hat{h}_i(p) * e^{\mp j\frac{2\pi n\xi}{N_{PN}}} \quad (8)$$

where N_{PN} denotes the length of PN sequence. $\hat{h}_i(p)$ represents the channel frequency response (CFR). The CFR is ex-

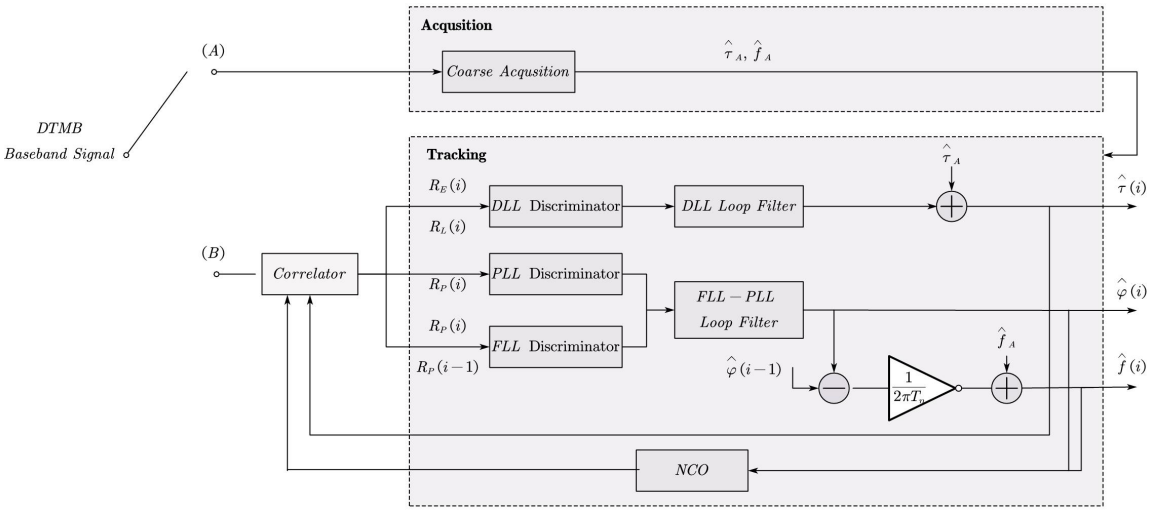

Figure 2. Overview of the proposed receiver

pressed as

$$\hat{h}_i(p) = \hat{x}_i x_i^*, i = 0, 1, 2, 3, ..., N_{CP} - 1 \tag{9}$$

where $\hat{x}_i$ is the received pilot symbol that has removed delay, frequency offset, and carrier phase estimate from the previous iteration of the tracking loops, which is shown in Fig. 2. x_i is the pilot symbols replica at the receiver. The normalized factor $k(\xi)$ is expressed as (Liu et al., 2022c)

$$k(\xi) = \frac{2A^2}{\pi^2 \xi^3}(1 - \cos 2\pi\xi - \pi\xi \sin 2\pi\xi) \tag{10}$$

where A is the received signal power.

3) Loop Filter: The loop filter includes the FLL-assisted PLL loop filter and the DLL loop filter. The FLL-assisted PLL loop filter is used to fuse the results from the FLL discriminator and the PLL discriminator. The FLL-assisted PLL loop filter structure is shown in Fig. 3. The FLL-assisted PLL loop filter is

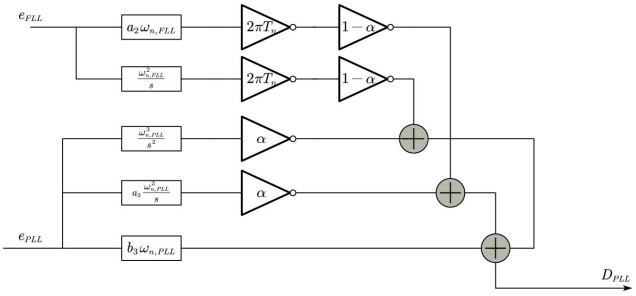

Figure 3. Loop Filter Structure For the FLL-Assisted PLL

expressed as

$$F_{FLL,PLL}(s) = b_3\omega_{n,PLL} + \alpha(a_3\frac{\omega_{n,PLL}^2}{s} + \frac{\omega_{n,PLL}^3}{s^2}) + (1-\alpha)(2\pi T_\eta)(a_2\omega_{n,FLL} + \frac{\omega_{n,FLL}^2}{s}) \tag{11}$$

where $\omega_{n,PLL}$ is the undamped natural frequency of the PLL loop, and $\omega_{n,FLL}$ is the undamped natural frequency of the FLL loop. The undamped natural frequency of the FLL loop, $\omega_{n,FLL}$, is related to the FLL noise-equivalent bandwidth $B_{n,FLL}$, and the relevant relationship is $B_{n,FLL} = \frac{1+a_2^2}{a_2}\omega_{n,FLL} = 0.53\omega_{n,FLL}$. $\omega_{n,PLL}$ is related to the PLL noise-equivalent bandwidth $B_{n,PLL}$, and the relevant relationship is $B_{n,PLL} = \frac{a_3 b_3^2 + a_3^2 - b_3}{4(a_3 b_3 - 1)}\omega_{n,PLL} = 0.7845\omega_{n,PLL}$ (Han et al., 2022). α represents the weight factor. The range of α is normally from 0 to 1, and the α is traditionally set as 0.5. The DLL loop filter is a normal 2-order loop filter, which is expressed as

$$F_{DLL}(s) = a_2\omega_{n,DLL} + \frac{\omega_{n,DLL}^2}{s} \tag{12}$$

where $\omega_{n,DLL}$ is the undamped natural frequency of the DLL loop, and the $\omega_{n,DLL}$ is related to the DLL noise-equivalent natural frequency of the DLL loop, the relevant relationship is $B_{n,DLL} = 0.53\omega_{n,DLL}$.

4. DTMB Positioning Framework

In this section, we utilized the extended Kalman filter (EKF) model to estimate the position. The mathematic model of the EKF is expressed as

$$\mathbf{x}_k = f(\mathbf{x}_{k-1}) + \mathbf{w}_k \tag{13}$$

$$\mathbf{z}_k = h(\mathbf{x}_k) + \mathbf{v}_k \tag{14}$$

where $\mathbf{x}_k \in \mathbb{R}^n$ is the state vector; $\mathbf{z}_k \in \mathbb{R}^n$ is the measurement vector provided by DTMB receiver proposed in this paper. The state vector $\mathbf{x}_k$ can be modeled as

$$\mathbf{x} = (\mathbf{p}, \mathbf{v}, c\delta t)^T \tag{15}$$

where $\mathbf{p} = (p_e, p_n)^T$ is the position in the 2 dimension planar, and $\mathbf{v} = (v_e, v_n)^T$ is the velocity in the 2 dimension planar. δt denotes the clock bias of the receiver, and c denotes the speed of the light. The measurement vector is expressed as

$$\mathbf{z} = (\rho_1, \rho_2, ..., \rho_n)^T \tag{16}$$

where ρ_i is the distance between the receiver and the ith DTMB station. n is the number of the DTMB stations. The calculation process of the EKF is as follows:

1) State Prediction: Calculate the one-step prediction of the

system state along with the associated covariance matrix of the prediction state estimation error, the process can be modeled as

$$\hat{\mathbf{x}}_{k|k-1} = f(\hat{\mathbf{x}}_{k-1}) = \Phi_{k-1}\hat{\mathbf{x}}_{k-1} \tag{17}$$

$$\Sigma_{k|k-1} = \Phi_{k-1}\Sigma_{k-1|k-1}\Phi_{k-1}^T + W_k \tag{18}$$

where $\Phi_{k-1} = \partial f/\partial x|_{x=\hat{\mathbf{x}}_{k-1}}$ is the Jacobian matrix; $\Sigma_{k|k-1} = \mathbb{E}(\mathbf{x}_k - \hat{\mathbf{x}}_{k|k-1})(\mathbf{x}_k - \hat{\mathbf{x}}_{k|k-1})^T$ is the state prediction error covariance matrix. W_k represents the state error matrix.

2) State Correction: Calculate the Kalman filter gain and update the state estimation, and the estimation error covariance matrix can be modeled as

$$K_k = \Sigma_{k|k-1}H_k^T(H_k\Sigma_{k|k-1}H_k^T + R_k)^{-1} \tag{19}$$

$$\hat{\mathbf{x}}_k = \hat{\mathbf{x}}_{k|k-1} + K_k[\mathbf{z}_k - h(\hat{\mathbf{x}}_{k|k-1})] \tag{20}$$

$$\Sigma_k = (I - K_kH_k)\Sigma_{k|k-1} \tag{21}$$

where $H_k = \partial h/\partial x|_{x=\hat{\mathbf{x}}_{k|k-1}}$. R_k is defined by the carrier-to-noise ratio (C/N0), and R_k can be expressed as

$$\mathrm{R}_k = \begin{pmatrix} 10^{-C/N0_1} & & & \\ & 10^{-C/N0_2} & & \\ & & \ddots & \\ & & & 10^{-C/N0_n} \end{pmatrix}_k \tag{22}$$

where $C/N0_i$ is the C/N0 (carrier-to-noise radio) of the ith DTMB station. The estimation of the C/N0 can be modeled as

$$C/N0 = 10\log_{10}(\frac{1}{T_\eta}\frac{\mu_P - 1}{M - \mu_P}) \tag{23}$$

where T_η denotes the integration time, and it equals with $T_\eta = \frac{1}{f_r}L_{frame}$. f_r is the resample rate, and f_r is set as 7.56 MHz. L_{frame} is the length of the frame, and it is set according to the signal model. For the model 1, L_{frame} is set as 4200, and for the model 3, L_{frame} is set as 4725. M represents the number of incoherent integrals, and it is set as 20 in this paper. μ_P is the mean of ratios for the narrow band power to width band power, and it can be modeled as

$$\mu_P = \frac{1}{K}\sum_{k=1}^{K}\frac{P_{nb}(k)}{P_{wb}(k)} \tag{24}$$

where K denotes the number of coherent integrals, and it is set as 5 in this paper. $P_{nb}(k)$ represents the narrow band power, and $P_{wb}(k)$ represents the width band power. The narrow band power $P_{nb}(k)$ and width band power $P_{wb}(k)$ can be calculated as

$$\begin{cases} P_{nb}(k) = (\sum_{n=KM+1}^{kM+M} I_{p,n})^2 + (\sum_{n=kM+1}^{kM+M} Q_{p,n})^2 \\ P_{wb}(k) = \sum_{n=KM+1}^{kM+M}[I_{p,n}^2 + Q_{p,n}^2] \end{cases} \tag{25}$$

where $R_{p,n} = I_{p,n} + jQ_{p,n}$ is the prompt correlation.

5. Experiment Setup and Receiver Configuration

In this section, we discuss the field experiment platform and the receiver configuration.

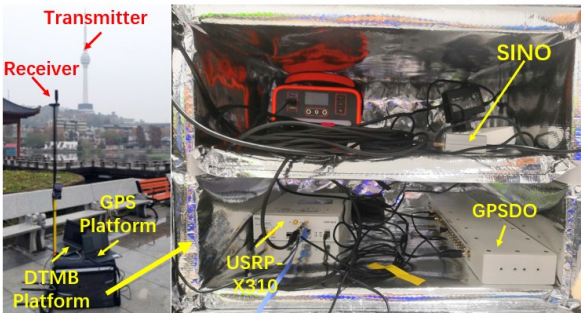

Figure 4. Experimental Platform for the Pedestrian Experiment

5.1 Experimental Setup

In this paper, we have conducted two experiments, including the pedestrian experiment and the on-vehicle experiment. For the pedestrian experiment, we utilized a bag equiped with a Universal Software Radio Peripheral (USRP) X310, a sino K803 GNSS receiver, and a global localization System Disciplined Oscillators (GPSDO), the platform for the pedestrian experiment is shown in Figure 4. About the on-vehicle experiment, we used a vehicle, and the vehicle also includes a USRP X310, a sino K803 GNSS receiver, and a GPSDO, and the vehicle is shown in Figure 5.

For these platform, the Sino K803 GNSS receiver is used to obtain GNSS observation. In this paper, we utilized the real-time kinematic (RTK) algorithm to process the obtained GNSS observation for the reference localization results. It shows that the horizontal accuracy of the reference localization results is less than 8mm, and the vertical accuracy is less than 15mm (Shen et al., 2022). The USRP X310 is used to collect the DTMB signal, and the GPSDO is utilized to provide a high-quality stable oscillator for the USRP devices. The output frequency of the GPSDO is 10MHz. The hold-over stability of the GPSDO is more than 25 μs.

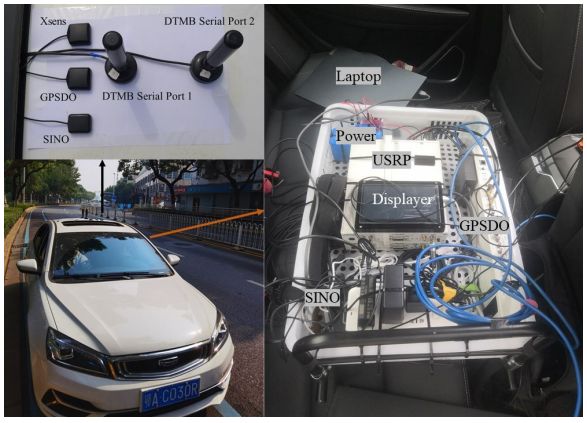

Figure 5. Experimental Platform for the on-Vehicle Experiment.

5.2 Receiver Configuration

The DTMB receiver is configured to process the received DTMB radio frequency (RF) signal for range detection. The bandwidth of the baseband stream is set to 8 MHz. The sampling rate of the baseband stream is set to 5 MHz, and the received signal would be resampled to 10 MHz. During the experiment, we collected the DTMB RF signal from 498 Mhz and 554 Mhz radio bands. The configuration of the DTMB receiver is summarized in Table 2. For the model 1 DTMB signal, the loop

integration time is set to $T_\eta \approx 555.6\mu s$ for DLL, FLL, and PLL. For the model 3 DTMB signal, the loop integration time is set to $T_\eta = 625\mu s$. We utilized the 2-order DLL, 2-order FLL, and 3-order PLL. The filter bandwidth is set to 10 Hz for both DLL and FLL, and the filter bandwidth is set to 30 Hz for PLL. The coefficient a_2 of the DLL and FLL is set to $a_2 = \sqrt{2}$. The coefficients a_3 and b_3 are set to 1.1 and 2.4, separately. The tracking threshold is set to 5 dB-Hz. If the current carrier-to-noise ratio is less than 5 dB-Hz, we will change the tracking status to unlock.

Table 2. DTMB Receiver Configuration

Base Configuration	
Carrier frequency f_c [MHz]	498, 554
Signal bandwidth B [MHz]	8
Sampling rate f_s [MHz]	5
Resampling rate f_r [Mhz]	10
Tracking Configuration	
DLL/ FLL/ PLL integration time T_η [μs] for model 1	555.6
DLL/ FLL/ PLL integration time T_η [μs] for model 3	625
DLL/ FLL/ PLL order	2,2,3
DLL/ FLL/ PLL bandwidth B_n [Hz]	10,10,30
DLL/ FLL filter coefficient a_2	$\sqrt{2}$
PLL filter coefficients a_3/b_3	1.1, 2.4
DLL nEML correlator half-spacing ξ	0.1
Unlocked Carrier-to-Noise Radio threshold	5 dB-Hz

6. Pedestrian Experiment

To evaluate the ranging performance of the designed DTMB receiver in this paper, we execute the pedestrian experiment near the DTMB station. The experiment scenario is shown in Figure 6.

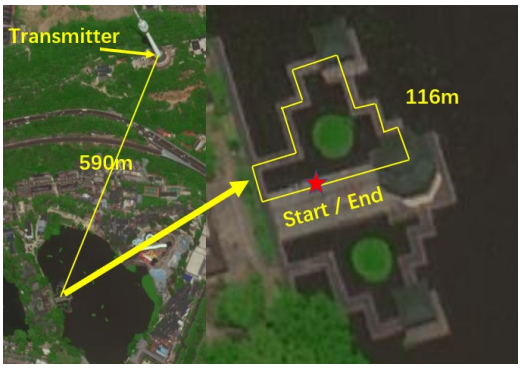

Figure 6. Pedestrian Experiment Scenario

The ranging results are shown in Figure 7. Figure 7 shows that the ranging results based on the DTMB carrier phase are very similar to the reference ranging results, and the accuracy static table is shown in Table 3. From Table 3, we observed that, under pedestrian environments, the RMSE (Root Mean Squared Error) of the ranging results from the carrier phase is 0.94m, and the $1-\sigma$ error is 0.94m. It shows that under pedestrian environments and the DTMB signal is well, the designed DTMB receiver can steadily provide sub-meter ranging results.

7. On-Vehicle Experiment

We have performed an on-vehicle experiment to evaluate the DTMB receiver's ranging and positioning performance in complex urban environments.

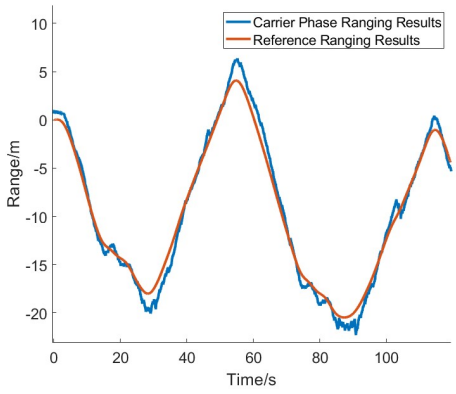

Figure 7. Detected Range Results from Carrier Phase under Pedestrian Environments

Table 3. Absolute Error Statistical Table of the Ranging Results based on the DTMB Carrier Phase

	Error of the Ranging Results
RMSE	0.94m
50% CDF	0.65m
68% CDF	0.94m

7.1 Experiment Scenario

The on-vehicle experiment scenario is shown in Figure 8. During the experimental stage, we collected the DTMB baseband signal from the CaiDian Station, the GuiShan Station, and the JiangXia Station. The distance between the CaiDian Station and the receiver is about 24 km, the distance between the GuiShan Station and the receiver is about 15 km, and the distance between the JiangXia Station and the receiver is about 12.7 km. In the experimental scenario, there are buildings, trees, and the high trestle bridge, and the experimental scenario is the typical urban environment.

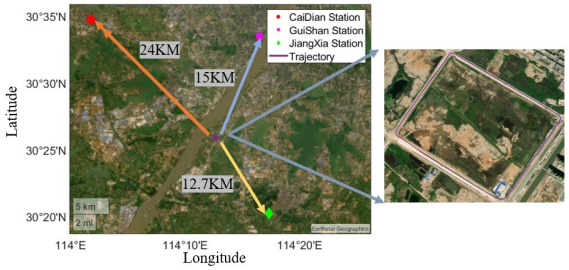

Figure 8. On-Vehicle Experimental Scenario.

7.2 Ranging Results

Although there is a higher accuracy for the carrier phase compared with the time-of-arrival (TOA), there is a lower robustness for the carrier phase, especially under complex environments or highly dynamic environments. For the GNSS position system, the ways to solve the problem include rebuilding the carrier phase and estimating integer ambiguity (Shen et al., 2022). However, these ways need the static reference station, and enough useful observations are normally more than 6. The on-vehicle experiment scenario does not have these conditions. Thus, we here utilized the range from the TOA for the position. In the complex urban environments, there are some stages that

the DTMB signal is very weak due to the NLOS environments. The fact will result in the receiver is unlocked. In principle, the C/N0 will be very low if the receiver is unlocked. The ranging results and the C/N0 from the CaiDian Station are shown in Figure 9.

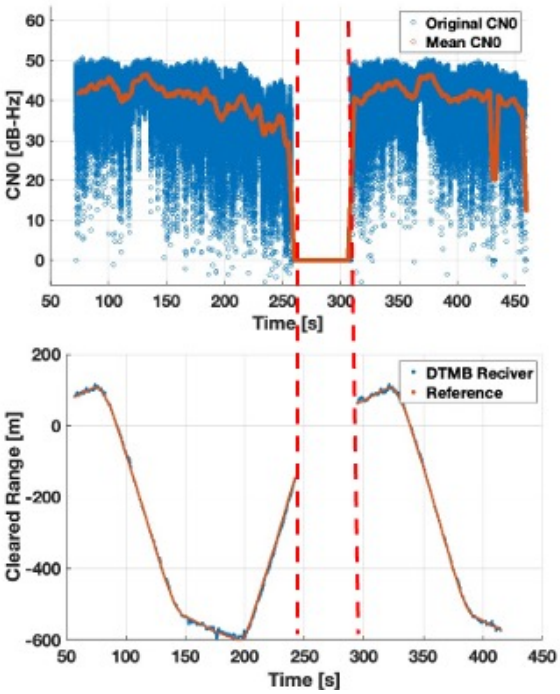

Figure 9. Detected Ranges and C/N0s Results from the CaiDian Station.

From Figure 9, we observed that the ranging results from the TOA are similar to the reference ranging results. We also found that the C/N0 during the unlocked stage is obviously less than in the locked stage, so we can remove the unusable measurements well based on the C/N0. The useful epochs' number of the CaiDian station signals accounts for 85.7% of the overall epochs, the useful epochs' number of the GuiShan station signals accounts for 95%, and the useful epochs' number of the JiangXia station signals accounts for 72.54% of the overall epochs. If the number of useful stations is more than 2, we can utilize the range observations for localization. Thus, the number of localizable epochs accounts for 92.24% of the overall epochs for this field experiment.

7.3 Localization results

The localization results are shown in Figure 10. As shown in Figure 10, we can arrive at a conclusion that the proposed receiver in the urban environments can provide relatively reliable localization results only based on the DTMB signal.

Table 4. Absolute Positioning Error Statistical Table

	Eastward	Northward
50% CDF	5.52m	4.07m
68% CDF	9.07m	7.74m

The localization errors are shown in Table 4. From Table 4, we observed that the 50% CDF(cumulative distribution function) of the positioning error in the eastward is 5.52m, the 50% CDF of the positioning error in the northward is 4.07m, the 68% CDF of the positioning error in the eastward is 9.07m, and the

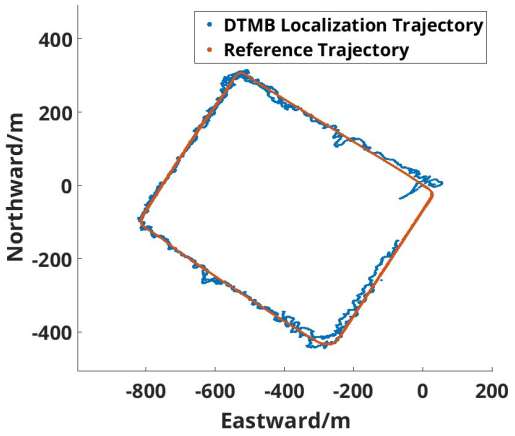

Figure 10. Localization Results

68% CDF of the positioning error in the northward is 7.74m. It means that the designed DTMB receiver can provide meter-level positioning results under complex urban environments and the relatively high dynamical environments. Reference (Wu et al., n.d.) shows that if the GNSS utilizes the TOA measurements, the $1-\sigma$ positioning error is about 16m. It means that the designed DTMB receiver can provide relatively reliable positioning results without using GNSS, and the positioning accuracy of the proposed DTMB receiver is approximate to the positioning accuracy based on the signal point positioning (SPP) method of the GNSS. Thus, the proposed DTMB receiver can be used as a non-GNSS-based PNT solution.

8. Conclusion

This paper has studied the wireless positioning in Chinese DTMB networks and proposed a DTMB receiver for positioning. A test scenario in the city of Wuhan has been considered to evaluate the performance of the proposed DTMB receiver. The pedestrian experiment results show that the designed receiver can provide sub-meter ranging results under pedestrian environments. The results of the on-vehicle experiment show that the designed receiver can provide meter-level positioning results in complex urban environments and relatively high dynamical environments.

In the future, work will focus on estimating the integer ambiguity of the DTMB carrier phase, fusing positioning methods based on the DTMB's TOA measurements and DTMB's carrier phase measurements, utilizing ML (machine learning) technology to obtain time-of-arrival estimation, as well as, integration with multi-sensor PNT systems to enhance robustness.

9. Acknowledgment

The research is supported by the National Natural Science Foundation of China (Grant No. 42171417), Guangxi Science and Technology Major Project (Grant No. AA22068072), and Jiangsu Province Science and Technology Major Special Project: Research and Development of Key Technologies for 6G Ubiquitous High-Precision Positioning (Grant num. BG2024003).

References

Chen, L., Julien, O., Thevenon, P., Serant, D., Peña, A. G., Kuusniemi, H., 2015. TOA Estimation for Positioning With

DVB-T Signals in Outdoor Static Tests. *IEEE Transactions on Broadcasting*, 61(4), 625-638.

Chen, L., Thevenon, P., Seco-Granados, G., Julien, O., Kuusniemi, H., 2016. Analysis on the TOA Tracking With DVB-T Signals for Positioning. *IEEE Transactions on Broadcasting*, 62(4), 957-961.

Han, Z., Liu, D., Wei, Z., Xu, Y., Li, R., 2022. A Carrier phase tracking method for vector tracking loops. *GPS Solutions*, 26. https://api.semanticscholar.org/CorpusID:251229776.

Hong, T., Sun, J., Jin, T., Yi, Y., Qu, J., 2021. Hybrid positioning with dtmb and lte signals. *2021 International Wireless Communications and Mobile Computing (IWCMC)*, 303–307.

Jiao, Z., Chen, L., Lu, X., Liu, Z., Zhou, X., Zhuang, Y., Guo, G., 2023. Carrier Phase Ranging with DTMB Signals for Urban Pedestrian Localization and GNSS Aiding. *Remote Sensing*, 15(2). https://www.mdpi.com/2072-4292/15/2/423.

Liu, X., Jiao, Z., Chen, L., Pan, Y., Lu, X., Ruan, Y., 2022a. An Enhanced Pedestrian Dead Reckoning Aided With DTMB Signals. *IEEE Transactions on Broadcasting*, 68(2), 407-413.

Liu, X., Liu, X., Jia, M., Li, F., Durrani, T. S., 2022b. Simultaneous Wireless Information and Power Transfer Based on Time–Frequency Block Allocation in OFDM Cooperative Communication System. *IEEE Systems Journal*, 16(3), 4827-4830.

Liu, Z., Chen, L., Zhou, X., Ruan, Y., Jiao, Z., Chen, R., 2022c. A PRECISE RANGING WITH SUBCARRIER DIVERSITY FOR 5G NR INDOOR POSITIONING. *The International Archives of the Photogrammetry, Remote Sensing and Spatial Information Sciences*, XLVI-3/W1-2022, 125-131.

Shen, N., Chen, L., Lu, X., Ruan, Y., Hu, H., Zhang, Z., Wang, L., Chen, R., 2022. Interactive multiple-model vertical vibration detection of structures based on high-frequency GNSS observations. *GPS Solut.*, 26(2). https://doi.org/10.1007/s10291-021-01215-x.

Wu, F., Wei, L., Luo, H., Zhao, F., Ma, X., Ning, B., n.d. T-SPP: Improving GNSS Single-Point Positioning Performance Using Transformer-Based Correction.

Wu, H., Wang, Q., Zhao, Y., Ma, X., Yang, M., Liu, B., Tang, R., Xu, X., 2016. Indoor localization using FM radio and DTMB signals. *Radio Science*, 51(7), 1030-1037.

Wu, Y., Hirakawa, S., Reimers, U., Whitaker, J., 2006. Overview of Digital Television Development Worldwide. *Proceedings of the IEEE*, 94(1), 8-21.

Yang, R., Zhan, X., Chen, W., Li, Y., 2022. An Iterative Filter for FLL-Assisted-PLL Carrier Tracking At Low C/N_0 and High Dynamic Conditions. *IEEE Transactions on Aerospace and Electronic Systems*, 58(1), 275-289.

Zhang, L., Li, W., Wu, Y., Hong, Z., Salehian, K., Wang, X., Angueira, P., Montalban, J., Velez, M., Park, S.-I., Kim, H. M., Lee, J.-Y., 2015. Performance Characterization and Optimization of Mobile Service Delivery in LDM-Based Next Generation DTV Systems. *IEEE Transactions on Broadcasting*, 61(4), 557-570.